Quantum quench dynamics in the Luttinger liquid phase of the Hatano-Nelson model

Balázs Dóra,[1,2,*] Miklós Antal Werner,[2,3,4] and Cătălin Paşcu Moca[4,5]
[1]*MTA-BME Lendület Topology and Correlation Research Group, Budapest University of Technology and Economics, Műegyetem rkp. 3, H-1111 Budapest, Hungary*
[2]*Department of Theoretical Physics, Institute of Physics, Budapest University of Technology and Economics, Műegyetem rkp. 3, H-1111 Budapest, Hungary*
[3]*Strongly Correlated Systems 'Lendület' Research Group, Wigner Research Centre for Physics, P.O. Box 49, 1525 Budapest, Hungary*
[4]*MTA-BME Quantum Dynamics and Correlations Research Group, Institute of Physics, Budapest University of Technology and Economics, Műegyetem rkp. 3, H-1111, Budapest, Hungary*
[5]*Department of Physics, University of Oradea, 410087 Oradea, Romania*

(Received 28 April 2023; accepted 21 June 2023; published 5 July 2023)

We investigate the quantum quench dynamics of the interacting Hatano-Nelson model with open boundary conditions using both Abelian bosonization and numerical methods. Specifically, we follow the evolution of the particle density and current profile in real space over time by turning the imaginary vector potential on or off in the presence of weak interactions. Our results reveal spatiotemporal Friedel oscillations in the system with light cones propagating ballistically from the open ends, accompanied by local currents of equal magnitude for both switch-off and -on protocols. Remarkably, the bosonization method accurately accounts for the density and current patterns with a single overall fitting parameter. The continuity equation is satisfied by the long-wavelength part of the density and current, despite the nonunitary time evolution when the Hatano-Nelson term is switched on.

DOI: 10.1103/PhysRevB.108.035104

I. INTRODUCTION

Non-Hermitian phenomena have been gaining significant attention in recent years, mainly due to their ability to exhibit unexpected features and their applicability to a broad range of classical and quantum systems [1,2]. These features include exceptional points [3–5], which refer to the points in the parameter space where two or more eigenvalues and eigenvectors of the matrix Hamiltonian coalesce. At these points the behavior of the system can change drastically. *PT* symmetry breaking [6] is another important feature of non-Hermitian systems, leading to the eigenvalues and eigenvectors becoming complex and the system becoming unstable, resulting in phenomena such as unidirectional invisibility, nonreciprocal energy transfer, and enhanced sensitivity. Additionally, non-Hermitian systems exhibit nontrivial topological phenomena, leading to the emergence of edge modes [7–17].

The Hatano-Nelson model is one of the earliest models in non-Hermitian physics [18,19]. It features noninteracting particles on a quantum ring, subject to an imaginary vector potential that renders the problem non-Hermitian. Initially, the focus was on persistent current and localization within this non-Hermitian context. However, this field has since experienced rapid expansion, with numerous studies being conducted on the non-Hermitian skin effect and related phenomena in the Hatano-Nelson model, as well as in other non-Hermitian systems such as photonic crystals [20,21] and electronic systems [22].

The non-Hermitian skin effect is characterized by the unusual localization of all eigenstates, as each single-particle eigenstate becomes exponentially localized at the boundaries of the system, even without the presence of disorder [12,23,24]. While this effect is primarily observed at the single-particle level, many studies have explored its behavior in a many-body context [25,26] using analytical Bethe ansatz [27,28], bosonization [29], and numerical methods [30–38]. However, the dynamics of the model, particularly in the interacting case, have received less attention. In Ref. [39] the evolution of the entanglement entropy and the transition from a volume to an area law in the noninteracting Hatano-Nelson model was studied during quantum quench dynamics, but fewer studies have investigated the dynamical properties of the interacting case.

Our motivation to investigate the quench dynamics of the interacting Hatano-Nelson model stems from the need to understand its dynamical properties, such as the propagation of the light cone and the spatiotemporal density and current profiles when the imaginary vector potential is turned on or off.

In general, in a quench problem, the initial state of the system is prepared in the ground state of the Hamiltonian with certain parameters, and then suddenly the parameters of the Hamiltonian are changed. This sudden change drives the system out of equilibrium, and the system's dynamics are governed by the new Hamiltonian. In general, non-Hermitian Hamiltonians may not have a well-defined ground state in the

*dora.balazs@ttk.bme.hu

traditional sense because they do not guarantee real eigenvalues or orthogonal eigenvectors. Instead, they often exhibit complex eigenvalues and nonorthogonal eigenvectors. Consequently, the concept of ground state, which relies on the lowest real eigenvalue and its corresponding eigenvector, is not directly applicable to non-Hermitian Hamiltonians. However, for some specific non-Hermitian systems such as the Hatano-Nelson model, the PT symmetry [6,40] guarantees that it has real eigenvalues and possesses a ground state.

To achieve this, we will employ bosonization, a powerful technique used to study low-dimensional systems, including one-dimensional systems of interacting fermions adapted to the non-Hermitian realm [29,41–44]. Additionally, we will use numerical tools like the density matrix renormalization group [45] (DMRG) to obtain the ground state and time-evolving block decimation (TEBD) [46] for analyzing the system's dynamics.

The structure of the paper is as follows: Section II provides an introduction to the bosonized version of the Hatano-Nelson model, including the construction of the vertex function, which enables the calculation of the spatiotemporal dependence of the average occupations. Sections IV and III are dedicated to the discussion of two types of quenches, in which the imaginary vector potential is either switched on or off. The relationship with the continuity equation is explored in Sec. V, and a comparison between the bosonization and numerical approaches is presented in Sec. VI.

II. BOSONIZED HATANO-NELSON MODEL

One can construct an effective low-energy Hamiltonian in the presence of an imaginary vector potential [29,47–49] using standard Abelian bosonization as

$$H = \int_0^L \frac{dx}{2\pi} v\left[K[\pi\Pi(x) - ih]^2 + \frac{1}{K}[\partial_x\phi(x)]^2\right], \quad (1)$$

where $\Pi(x)$ and $\phi(x)$ are the dual fields satisfying the regular commutation relation [48], $[\Pi(x), \phi(x')] = i\delta(x - x')$. This non-Hermitian Hamiltonian is brought to conventional Luttinger liquid (LL) form by applying a similarity transformation [29], which eliminates the vector potential terms using $S^{-1}HS$, with

$$S = \exp\left(\frac{h}{\pi}\int_0^L \phi(x')dx'\right), \quad (2)$$

and S^{-1} is obtained from S after the $h \to -h$ change. The resulting Hamiltonian is diagonalized after introducing canonical bosonic fields [47,50] as

$$H_b = \sum_{q>0} \omega(q) b_q^\dagger b_q, \quad (3)$$

and the long-wavelength part of the local charge density is $\partial_x\phi(x)/\pi$, with

$$\phi(x) = i\sum_{q>0}\sqrt{\frac{\pi K}{qL}}\sin(qx)[b_q - b_q^\dagger] \quad (4)$$

for open boundary conditions (OBCs) [51]. K is the LL parameter [47], which carries all the nonperturbative effects of interaction, and $\omega(q) = vq$, with v the Fermi velocity in the interacting systems and $q = l\pi/L$ with $l = 1, 2, 3\ldots$. From Eq. (3), the model has *gapless* and *real* spectra within the realm of open boundary bosonizaton; only the Fermi velocity can get renormalized by both interactions and imaginary vector potential. Therefore, when studying quantum quenches, the spectrum retains its essential characters. The ground state of Hamiltonian (3) is the bosonic vacuum $|0\rangle$, and the ground state of the original non-Hermitian Hamiltonian (1) is obtained by applying S to the vacuum state $|0\rangle$:

$$|\Phi\rangle = \frac{S|0\rangle}{\sqrt{\langle 0|S^2|0\rangle}}, \quad (5)$$

where in the denominator we use the Hermiticity of S as defined in Eq. (2). This indicates that the low-energy effective theory of the interacting Hatano-Nelson model is a Luttinger liquid with collective bosonic excitations, similarly to Hermitian systems [47,51,52].

We investigate the vertex operator [53], given by

$$G_\lambda(x,t) = \langle\Phi(t)|\exp[i\lambda\phi(x)]|\Phi(t)\rangle, \quad (6)$$

where $|\Phi(t)\rangle$ is the time-evolved wave function after the quench, as we discuss below. From this, the long wavelength and $2k_F$ oscillating part of the density are obtained as

$$n_0(x,t) = \frac{1}{\pi}\lim_{\lambda\to 0}\partial_x G_\lambda(x,t)/(i\lambda), \quad (7a)$$

$$n_{2k_f}(x,t) = G_2(x,t). \quad (7b)$$

For the quench problems that we address, we are able to provide analytical expression for the vertex function in Eq. (6) and consequently, for the time-dependent particle densities.

III. SWITCHING OFF THE NON-HERMITIAN TERM ($h \neq 0 \to h = 0$)

In the first configuration we prepare the system in the ground state as defined by Eq. (5) with an imaginary vector potential present. The quench consists in turning off the vector potential and allowing the system to evolve unitarily under the Hermitian Hamiltonian (36) with zero imaginary vector potential, $h = 0$ [54]. We coin this as the "switch-off" protocol. The time evolution is therefore

$$|\Phi(t)\rangle = \frac{\exp(-iH_b t)S|0\rangle}{\sqrt{\langle 0|S^2|0\rangle}}. \quad (8)$$

The vertex operator is evaluated by realizing that for any A and B, two operators that are linear in the bosonic field, such as, for example, in Eq. (4), the identity

$$\exp(A)\exp(B)\exp(A) = \exp(2A + B) \quad (9)$$

holds. (Its derivation follows from using the Baker-Campbell-Hausdorff formula [53] twice.) Then eventually we get

$$G_\lambda(x,t) = \frac{\langle 0|\exp(i\lambda\phi(x,t) + \frac{2h}{\pi}\int_0^L \phi(x')dx')|0\rangle}{\langle 0|\exp\left(\frac{2h}{\pi}\int_0^L \phi(x')dx'\right)|0\rangle}, \quad (10)$$

where $\phi(x,t) = \exp(iH_b t)\phi(x)\exp(-iH_b t)$ is the time-dependent bosonic field. This amounts to using $b_q(t) = b_q\exp[-i\omega(q)t]$ and $b_q^\dagger(t) = b_q\exp[i\omega(q)t]$ in Eq. (4).

Using the standard trick of $\langle\exp(A)\rangle = \exp(\langle A^2\rangle/2)$, which is valid for a Gaussian wave function and an operator A being

linear in the bosonic field, the expectation value of the vertex operator is evaluated to yield

$$\ln G_\lambda(x,t) = -\frac{\lambda^2}{2}\langle 0|\phi(x,t)^2|0\rangle + \frac{ih\lambda L}{\pi}\int_0^L \frac{dx'}{L}\langle 0|\{\phi(x,t),\phi(x')\}|0\rangle, \quad (11)$$

where the expectation values can be easily evaluated [47], and $\{A,B\}$ denotes the anticommutator. Altogether, it is rewritten as

$$\ln G_\lambda(x,t) = -\frac{\lambda^2}{2}C_\phi(x) + \frac{2i\lambda hL}{\pi}g(x,t), \quad (12)$$

with

$$C_\phi(x) = \langle 0|\phi(x,t)^2|0\rangle = \frac{K}{2}\ln\left[\frac{2L}{\pi\alpha}\sin\left(\frac{\pi x}{L}\right)\right] \quad (13)$$

being time independent, since $\exp(-iH_b t)|0\rangle = |0\rangle$, and valid for $\alpha \ll x \ll L$ with α as the short-distance cutoff, a remnant of the lattice constant when taking the continuum limit. The second term involving the anticommutator gives

$$g(x,t) \equiv \int_0^L \frac{dx'}{2L}\langle 0|\{\phi(x,t),\phi(x')\}|0\rangle = \frac{K}{2\pi}\,\mathrm{Im}\sum_{\beta,\sigma=\pm}\beta\,\mathrm{polylog}\left[2,\beta\exp\left(\frac{i\pi(x+\sigma vt)}{L}\right)\right], \quad (14)$$

where polylog $(2,x)$ is the second-order polylogarithm [55]. This is valid in the scaling limit, when the space-time parameters x and vt and their combinations, including the light cones at $x \pm vt$, differ significantly from α and L. The $g(x,t)$ function is periodic in both x and vt with period $2L$. The expectation value of the vertex operator, $G_\lambda(x,t)$, is also related to the generating function of the quantity ϕ. It features the usual contribution from a LL with open boundary condition, $C_\phi(x)$, and an additional piece coming from the Hatano-Nelson term, $g(x,t)$. As we show below, similar properties characterize the dual field Θ as well. In Fig. 1 we plot the function $g(x,t)$, which captures all effect of non-Hermiticity within the validity of a low-energy theory.

The homogeneous part of the particle density exhibits ballistic propagation of the initial non-Hermitian-parameter–induced density profile as

$$n_0(x,t) = -\frac{Kh}{\pi^2}\sum_{\sigma=\pm}\ln\left|\tan\left(\frac{\pi(x+\sigma vt)}{2L}\right)\right|, \quad (15)$$

and is directly proportional to $\partial_x g(x,t)$ through Eq. (7a). Initially, light cones appear at and around the boundaries of the system and start propagating to the other ends with time. For $vt = L(k+\frac{1}{2})$ with integer k, this homogeneous part vanishes identically, and we are left only with the $2k_F$ oscillating part of the density, as shown in Fig. 2. Putting everything together,

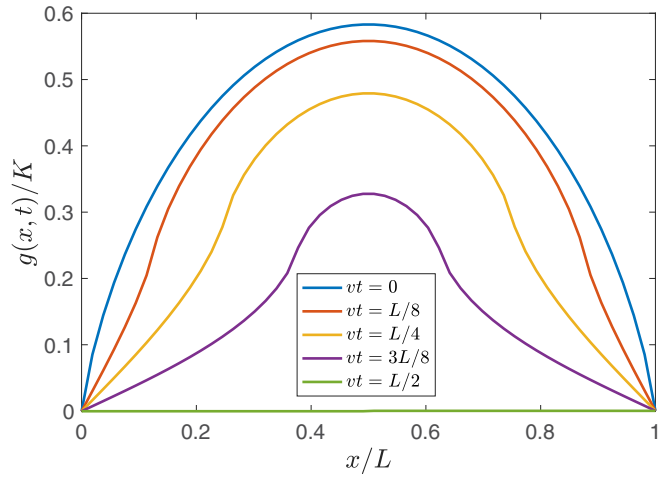

FIG. 1. The time evolution of $g(x,t)$ from Eq. (14) is visualized, carrying all the effects of the Hatano-Nelson term for the quarter-time period. For longer times it exhibits a sign change before reverting to the above pattern.

the total time-dependent particle density is

$$\rho(x,t) = \rho_0 + n_0(x,t) + c\left(\frac{\pi\alpha}{2L\sin\left(\frac{\pi x}{L}\right)}\right)^K \sin\left(2k_F x - \frac{4hL}{\pi}g(x,t) + \delta\right), \quad (16)$$

where ρ_0 represents the homogeneous background, c is an overall constant, which cannot be obtained from the low-energy theory, and δ denotes the phase shift.

The redistribution of charge is accompanied by local currents flowing in the system. Their effect can be captured by evaluating the other vertex operator,

$$F_\lambda(x,t) = \langle\Phi(t)|\exp\left[i\lambda\Theta(x)\right]|\Phi(t)\rangle, \quad (17)$$

where

$$\Theta(x) = \sum_{q>0}\sqrt{\frac{\pi}{KqL}}\cos(qx)[b_q + b_q^\dagger]. \quad (18)$$

Within the low-energy effective theory, the $2k_f$ oscillating part of the particle current is usually highly irrelevant (its scaling dimension is large compared to its long-wavelength counterpart), and therefore we refrain from analyzing it. This yields the local current [47] through

$$j_0(x,t) = \frac{vK}{\pi}\lim_{\lambda\to 0}\partial_x F_\lambda(x,t)/(i\lambda). \quad (19)$$

Following similar steps, we obtain

$$\ln F_\lambda(x,t) = -\frac{\lambda^2}{2}C_\Theta(x) + \frac{2ih\lambda L}{\pi}f(x,t), \quad (20)$$

where

$$C_\Theta(x) = \langle 0|\Theta(x,t)^2|0\rangle = -\frac{1}{2K}\ln\left[\frac{2\pi\alpha}{L}\sin\left(\frac{\pi x}{L}\right)\right] \quad (21)$$

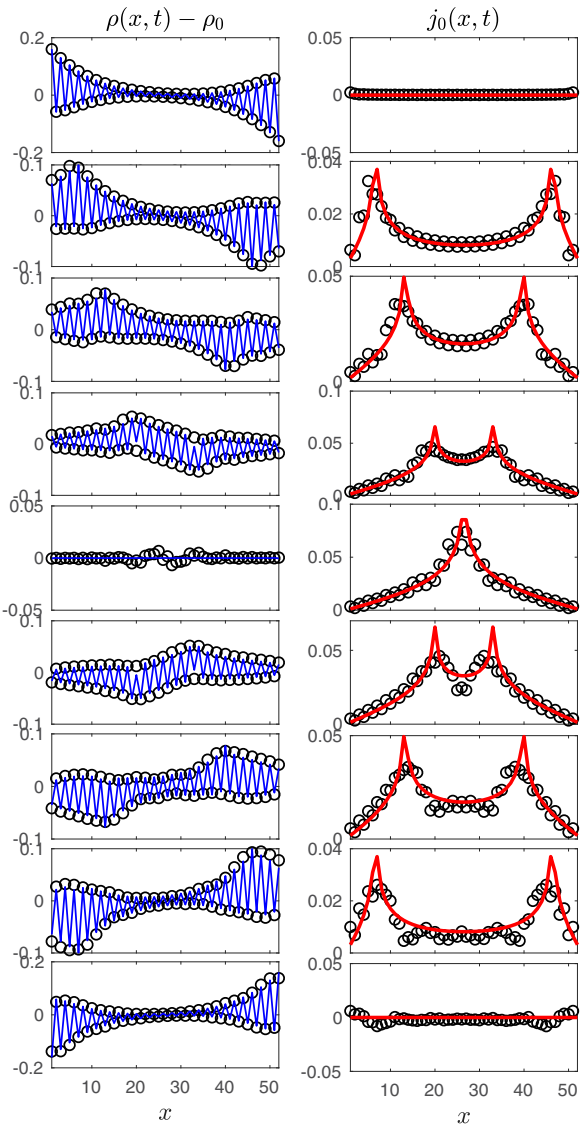

FIG. 2. Real-space density profile (left) and current (right) for the interacting Hatano-Nelson model with $U = 0.5J$, $L = 52$, and times $t = kL/8v$, with $k = 0 : 1 : 8$ from top to bottom after switching off $h = 0.1$. The Friedel oscillations are plotted using $c = 0.42$ and $\delta = 0$. The circles denote the numerical data from DMRG, the only overall fitting parameter is c for the oscillating part of the particle density, and the long-wavelength parts contain no fitting parameter, as seen from Eqs. (15) and (23).

is time independent. The other function $f(x,t)$ is found to be related to $g(x,t)$ from the particle density as

$$f(x,t) \equiv \int_0^L \frac{dx'}{2L}\langle 0|\{\Theta(x,t),\phi(x')\}|0\rangle = -\frac{g(vt,x/v)}{K}, \tag{22}$$

which is independent from the LL parameter K, since the two bosonic fields get renormalized in an opposite fashion in Eqs. (4) and (18). This gives

$$j_0(x,t) = \frac{vhK}{\pi^2}\sum_{\sigma=\pm}\sigma \ln\left|\tan\left(\frac{\pi(x+\sigma vt)}{2L}\right)\right|, \tag{23}$$

which vanishes at $t = 0$ as expected. It exhibits light cones similarly to the particle density.

IV. SWITCHING ON THE NON-HERMITIAN TERM ($h = 0 \to h \neq 0$)

In the alternative protocol, we follow the reverse procedure, starting from the Hermitian ground state with no imaginary vector potential ($h = 0$), and then abruptly switch on the non-Hermitian parameter h. This results in a true non-Hermitian quench, as the time evolution becomes nonunitary due to the presence of the imaginary vector potential. Here the initial state is the bosonic vacuum $|0\rangle$, and the time evolution is dictated by Eq. (1), which can be expressed using the inverse similarity transformation as SH_bS^{-1}. This will be dubbed the "switch-on" protocol. The time-evolved wave function is then

$$|\Phi(t) = \frac{S\exp(-iH_bt)S^{-1}|0\rangle}{\sqrt{\langle 0|S^{-1}\exp(iH_bt)S^2\exp(-iH_bt)S^{-1}|0\rangle}}. \tag{24}$$

Using Eq. (9) twice and the time evolution, we get

$$G_\lambda(x,t) = \frac{\langle 0|\exp\left(i\lambda\phi(x,t) + \frac{2h}{\pi}\int_0^L[\phi(x',t)-\phi(x')]dx'\right)|0\rangle}{\langle 0|\exp\left(\frac{2h}{\pi}\int_0^L[\phi(x',t)-\phi(x')]dx'\right)|0\rangle}. \tag{25}$$

After taking the expectation value, this reads as

$$\ln G_\lambda(x,t) = -\frac{\lambda^2}{2}\langle 0|\phi(x,t)^2|0\rangle + \frac{ih\lambda L}{\pi}\int_0^L\frac{dx'}{L} \times \langle 0|\{\phi(x,t),\phi(x',t)-\phi(x')\}|0\rangle, \tag{26}$$

which differs from Eq. (11) by the equal-time autocorrelator $\sim\int_0^L\langle 0|\{\phi(x,t),\phi(x',t)\}|0\rangle dx'$, which is independent of time. Putting everything together, we obtain

$$\ln G_\lambda(x,t) = -\frac{\lambda^2}{2}C_\phi(x) + \frac{2ih\lambda L}{\pi}[g(x,0)-g(x,t)]. \tag{27}$$

The homogeneous part of the particle density builds up as

$$n_0(x,t) = -\frac{Kh}{\pi^2}\left(2\ln\left[\tan\left(\frac{\pi x}{2L}\right)\right] - \sum_{\sigma=\pm}\ln\left|\tan\left(\frac{\pi(x+\sigma vt)}{2L}\right)\right|\right). \tag{28}$$

Combining all elements, the overall time-dependent particle density is

$$\rho(x,t) = \rho_0 + n_0(x,t) + c\left(\frac{\pi\alpha}{2L\sin\left(\frac{\pi x}{L}\right)}\right)^K \times \sin\left(2k_Fx + \frac{4hL}{\pi}[g(x,t)-g(x,0)]\right), \tag{29}$$

where ρ_0 represents the homogeneous background. These are plotted in Figs. 3 and 4. These results indicate that at least for small h, the strong localization of eigenstates to one end of the chains through the non-Hermitian skin effect does not appear, but rather, a ballistic propagation of light cones characterizes the dynamics.

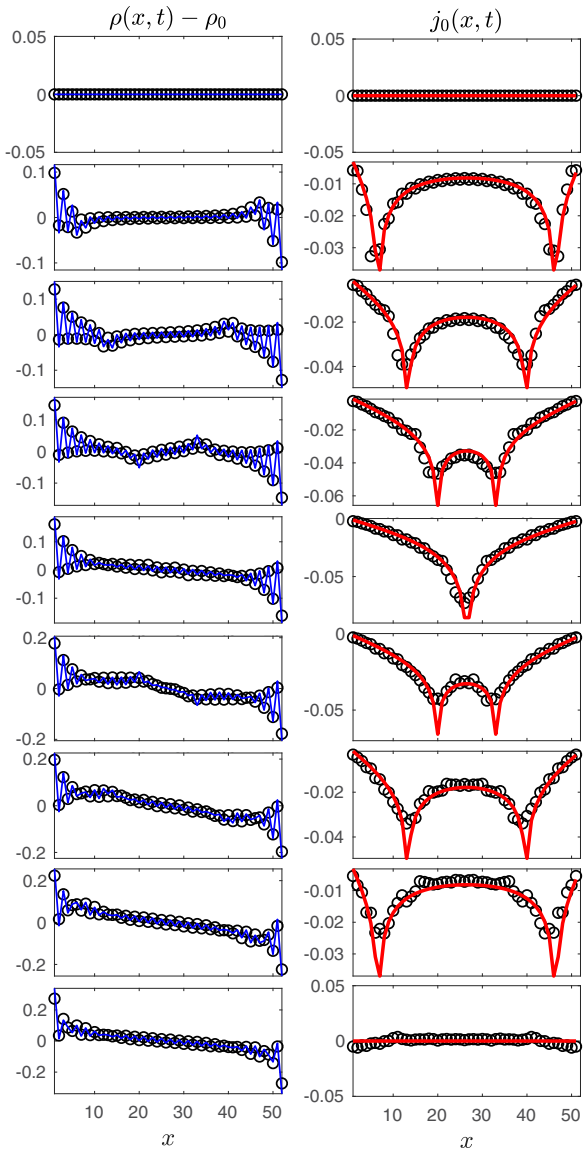

FIG. 3. Real-space density profile (left) and current (right) for the noninteracting case with $U=0$, $L=52$, and times $t=kL/8v$, with $k=0:1:8$ from top to bottom after switching on $h=0.1$. The Friedel oscillations are plotted using $c=0.43$ and $\delta=0$. The circles denote the tight-binding numerics, the only overall fitting parameter is c for the oscillating part of the particle density, and the long-wavelength parts contain no fitting parameter, as expected from Eqs. (28) and (32).

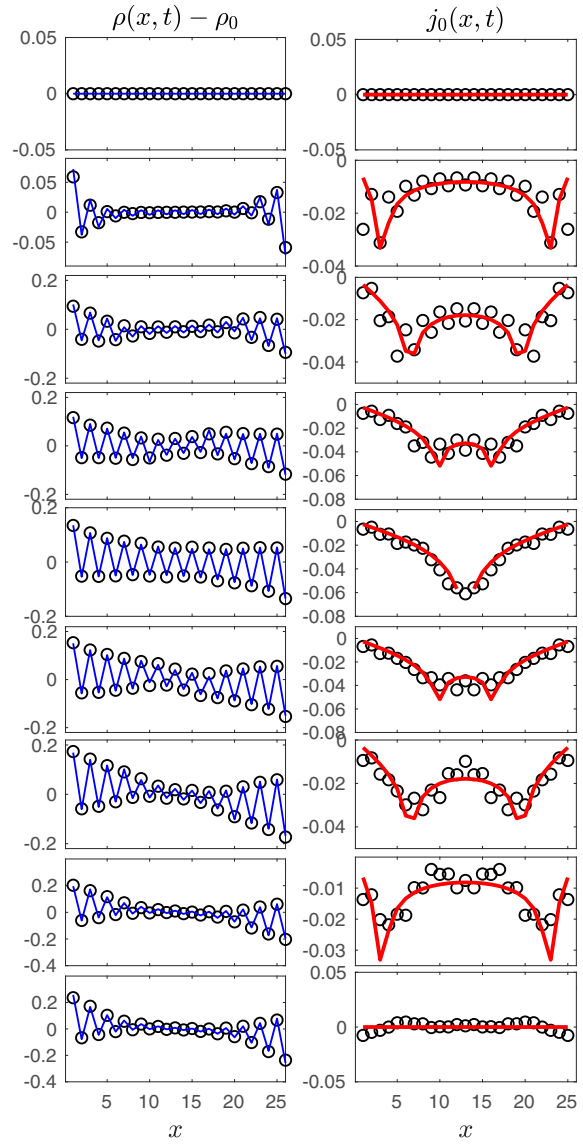

FIG. 4. Real-space density profile (left) and current (right) for the interacting case with $U=0.5J$, $L=26$, and times $t=kL/8v$, with $k=0:1:8$ from top to bottom after switching on $h=0.1$. The Friedel oscillations are plotted using $c=0.43$ and $\delta=0$. The circles denote the many-body ED results, the only overall fitting parameter is c for the oscillating part of the particle density, and the long-wavelength parts contain no fitting parameter, in accordance with Eqs. (28) and (32).

We have also evaluated the current after switching on the non-Hermitian term. For the generating function, we obtain

$$F_\lambda(x,t)=\frac{\langle 0|\exp\left(i\lambda\Theta(x,t)+\frac{2h}{\pi}\int_0^L[\phi(x',t)-\phi(x')]dx'\right)|0\rangle}{\langle 0|\exp\left(\frac{2h}{\pi}\int_0^L[\phi(x',t)-\phi(x')]dx'\right)|0\rangle}. \tag{30}$$

After taking the expectation value, we get a term of the form $\langle 0|\{\Theta(x,t),\phi(x',t)-\phi(x')\}|0\rangle$. From this, the equal-time anticommutator vanishes identically in the ground state, i.e., $\langle 0|\{\Theta(x,t),\phi(x',t)\}|0\rangle=\langle 0|\{\Theta(x),\phi(x')\}|0\rangle=0$. Then, we get

$$\ln F_\lambda(x,t)=-\frac{\lambda^2}{2}C_\Theta(x)-\frac{2ih\lambda L}{\pi}f(x,t), \tag{31}$$

where $C_\Theta(x)$ and $f(x,t)$ are given by Eqs. (21) and (22). This yields

$$j_0(x,t)=-\frac{vhK}{\pi^2}\sum_{\sigma=\pm}\sigma\ln\left|\tan\left(\frac{\pi(x+\sigma vt)}{2L}\right)\right|, \tag{32}$$

which is identical to the previous case (except for an overall minus sign) when the non-Hermitian term is switched off. The ensuing density and current pattern is very similar to that

in Fig. 2, albeit the particle density picks up an additional time-independent tilt from the first term on the right-hand side of Eq. (28), while the current simply flows in the opposite direction compared to Fig. 2.

V. CONTINUITY EQUATION

The continuity equation states that the local density changes in time when local currents flow or some external source or sink is present [56]. By decomposing the non-Hermitian Hamiltonian as $H = H_0 + iV$ with both H_0 and V Hermitian, the expectation value of the local density n is

$$\langle n\rangle = \frac{\langle\Phi(t)|n|\Phi(t)\rangle}{\langle\Phi(t)|\Phi(t)\rangle}, \tag{33}$$

where $|\Phi(t)\rangle = e^{-iHt}|\Phi_0\rangle$. The time derivative of this expectation value reads as [57]

$$\partial_t\langle n\rangle = i\langle[H,n]\rangle + \langle\{V,n\}\rangle - 2\langle n\rangle\langle V\rangle, \tag{34}$$

where $[A,B]$ stands for the commutator. The first term on the right-hand side represents the conventional term for Hermitian systems; the second term with the anticommutator stems from the non-Hermitian contribution, namely, from the interaction with the environment; while the very last term originates from the explicit normalization of the wave function in Eq. (33). Then the continuity equation is

$$\partial_t\langle n\rangle + \partial_x\langle j\rangle = \langle\{V,n\}\rangle - 2\langle n\rangle\langle V\rangle. \tag{35}$$

For the "switch-off" protocol, the time evolution is dictated by a Hermitian Hamiltonian; thus $V = 0$ and the continuity equation holds naturally, as expected. For the switch-on procedure, on the other hand, $V = -vhK\int_0^L \Pi(x)dx = vhK[\Theta(0) - \Theta(L)]/\pi$ from Eq. (1). Using this and the long-wavelength density operator $n = \partial_x\phi(x)/\pi$, the right-hand side of Eq. (35) indeed vanishes, in accordance with Eqs. (28) and (32), which makes the left hand of Eq. (35) vanish.

VI. NUMERICS

The Hatano-Nelson model [18,19] consists of fermions hopping in one dimension in the presence of an imaginary vector potential. The interacting many-body version of the Hamiltonian is

$$H_{HN} = \sum_{n=1}^{N-1}\frac{J}{2}\exp(ah)c_n^\dagger c_{n+1} + \frac{J}{2}\exp(-ah)c_{n+1}^\dagger c_n + Uc_n^\dagger c_n c_{n+1}^\dagger c_{n+1}, \tag{36}$$

where $J > 0$ is the uniform hopping; h is the constant imaginary vector potential and a represents the lattice constant; N is the total number of lattice sites and we consider an open boundary condition (OBC); and U represents the nearest-neighbor interaction between particles. The first term describes the hopping of particles from site n to site $n+1$, while the second term describes the opposite hopping direction. We consider half filling with $N/2$ fermions populating the lattice. The model is PT symmetric [40] and possesses a real spectrum for OBC, and the minimal energy configuration is the ground state with a many-body wave function $|\Psi\rangle$. In the presence of finite U, the LL parameter is $K = \pi/2/[\pi - \arccos(U/J)]$, while v can be obtained from the $2L/v$ time periodicity of the density and current patterns. More precisely, the current vanishes identically for the first time after the switch on or off at $t = L/v$. We assume that the above value of K remains valid also for small h as well. We expect bosonization to remain valid for larger values of h, albeit for this case, no explicit expression is available for the h and U dependence of the LL parameter K; therefore it should be treated as a free fitting parameter when comparing bosonization to numerical data.

Equation (36) has a real spectrum for any ah parameter. However, as $ah \to \infty$, the spectrum of the noninteracting model softens. In the $ah = \infty$ limit, the spectrum of the noninteracting model becomes completely flat and contains N zero-energy modes. Due to the lack of any nonzero Fermi velocity, bosonization cannot be applied in this limit. Moreover, when the right and left hopping processes acquire different signs, the spectrum becomes complex due to PT symmetry breaking. Consequently, there is no similarity transformation S mapping the non-Hermitian model to a Hermitian one, and our current approach is not expected to work for that scenario. Let us note that bosonization is expected to capture additional deformations of the noninteracting spectrum as well, such as starting from a non-Hermitian SSH model or with next-nearest-neighbor non-Hermitian hoppings as well.

We study H_{HN} numerically by solving the time-dependent Schrödinger equation for $U = 0$. The initial many-body (i.e., $N/2$-body) state Ψ_0 is a Slater determinant made from the single-particle eigenstates of Eq. (36) as ϕ_n with $h \neq 0$, but $\langle\phi_n|\phi_n'\rangle \neq \delta_{n,n'}$ due to non-Hermiticity. Then, the switch-off protocol is followed at the single-particle level as $\phi_n(t) = \exp[-iH_{HN}t]\phi_n$ for $t > 0$ with $h = 0$ in H_{HN}. The switch-on protocol is slightly different: The initial wave functions are orthogonal due to the $h = 0$ Hermitian initial Hamiltonian as $\langle\phi_n|\phi_n'\rangle = \delta_{n,n'}$. They become nonorthogonal only due to the nonunitary time evolution from $h \neq 0$. The corresponding results are shown in Fig. 3.

The time-evolved many-body wave function $\Psi(t)$ remains a Slater determinant built up from these time-dependent single-particle functions, which are not orthogonal for both protocols. After time t, we evaluate numerically the change in the density profile [1,58,59] as

$$\rho(n,t) = \frac{\langle\Psi(t)|c_n^\dagger c_n|\Psi(t)\rangle}{\langle\Psi(t)|\Psi(t)\rangle}, \tag{37}$$

where the denominator is required, as it accounts for the nonunit norm of the many-body wave function [57], and the homogeneous background density is $\rho_0 = 1/2$. For the switch-off protocol, this differs from unity but does not change in time, while for the switch-on protocol, it would start from unity and change with time. Since the many-body wave function is a Slater determinant, c_n in the numerator acts separately on the single-particle wave functions. However, due to the nonorthogonality of $\phi_n(t)$, the overlap of the other wave functions, not acted on by c_n, has to be evaluated as well and can give a nontrivial (i.e., not 0 or 1) contribution. We also evaluate in a similar fashion the time-evolved local particle current operator from

$$j_n = iJ(c_{n+1}^\dagger c_n - c_n^\dagger c_{n+1})/2. \tag{38}$$

When dealing with finite U, we use many-body exact diagonalization (ED) on small systems (Fig. 4). We also utilize the DMRG algorithm [60] to search for the many-body ground state within the matrix product states (MPS) framework. Subsequently, the MPS wave function $\Psi(t)$ is time evolved, and the density and current profiles are calculated as described in Eq. (37); see Fig. 3 as well. In the switch-off approach, the time evolution is unitary, and the wave function maintains its normalization at any later time. Conversely, in the switch-on protocol, the wave function is no longer normalized due to the nonunitary evolution.

VII. CONCLUSIONS

Our research focused on examining the behavior of the many-body interacting Hatano-Nelson model with open boundary condition following a quantum quench. Using Abelian bosonization, we derived analytical expressions for the spatiotemporal profiles of both density and current along the chain. Two distinct quench protocols were considered, one with a unitary evolution after switching off the non-Hermitian term and one with a nonunitary evolution after switching on the imaginary vector potential. Our findings revealed that in both cases, the dynamics exhibited a ballistic behavior of light-cone propagation, starting from the ends of the chain. This influenced the homogeneous particle density, the Friedel oscillations, as well as the particle current. The continuity equation involving the long-wavelength part of the density and current remains satisfied, in spite of non-Hermiticity [56]. Interestingly, we found that the magnitude of the current is the same for both protocols. Our results were supported by numerical methods, such as exact diagonalization or time-evolving block decimation.

ACKNOWLEDGMENTS

This research is supported by the National Research, Development and Innovation Office – NKFIH within the Quantum Technology National Excellence Program (Project No. 2017-1.2.1-NKP-2017-00001), No. K134437, No. K142179, by the BME-Nanotechnology FIKP grant (BME FIKP-NAT), and by a grant of the Ministry of Research, Innovation and Digitization, CNCS/CCCDI-UEFISCDI, under Project No. PN-III-P4-ID-PCE-2020-0277 and under the Project for Funding the Excellence, Contract No. 29 PFE/30.12.2021. M.A.W. has also been supported by the Janos Bolyai Research Scholarship of the Hungarian Academy of Sciences and by the ÚNKP-22-5-BME-330 New National Excellence Program of the Ministry for Culture and Innovation from the source of the National Research, Development and Innovation Fund.

[1] Y. Ashida, Z. Gong, and M. Ueda, Non-Hermitian physics, Adv. Phys. **69**, 249 (2020).
[2] E. J. Bergholtz, J. C. Budich, and F. K. Kunst, Exceptional topology of non-Hermitian systems, Rev. Mod. Phys. **93**, 015005 (2021).
[3] W. D. Heiss, The physics of exceptional points, J. Phys. A: Math. Theor. **45**, 444016 (2012).
[4] H. Hodaei, A. U. Hassan, S. Wittek, H. Garcia-Gracia, R. El-Ganainy, D. N. Christodoulides, and M. Khajavikhan, Enhanced sensitivity at higher-order exceptional points, Nature (London) **548**, 187 (2017).
[5] K. Ding, C. Fang, and G. Ma, Non-Hermitian topology and exceptional-point geometries, Nat. Rev. Phys. **4**, 745 (2022).
[6] R. El-Ganainy, K. G. Makris, M. Khajavikhan, Z. H. Musslimani, S. Rotter, and D. N. Christodoulides, Non-Hermitian physics and PT symmetry, Nat. Phys. **14**, 11 (2018).
[7] I. Rotter and J. P. Bird, A review of progress in the physics of open quantum systems: Theory and experiment, Rep. Prog. Phys. **78**, 114001 (2015).
[8] T. Gao, E. Estrecho, K. Y. Bliokh, T. C. H. Liew, M. D. Fraser, S. Brodbeck, M. Kamp, C. Schneider, S. Höfling, Y. Yamamoto, F. Nori, Y. S. Kivshar *et al.*, Observation of non-Hermitian degeneracies in a chaotic exciton-polariton billiard, Nature (London) **526**, 554 (2015).
[9] L. Zhou, Q.-h. Wang, H. Wang, and J. Gong, Dynamical quantum phase transitions in non-Hermitian lattices, Phys. Rev. A **98**, 022129 (2018).
[10] J. M. Zeuner, M. C. Rechtsman, Y. Plotnik, Y. Lumer, S. Nolte, M. S. Rudner, M. Segev, and A. Szameit, Observation of a Topological Transition in the Bulk of a Non-Hermitian System, Phys. Rev. Lett. **115**, 040402 (2015).
[11] Z. Gong, Y. Ashida, K. Kawabata, K. Takasan, S. Higashikawa, and M. Ueda, Topological Phases of Non-Hermitian Systems, Phys. Rev. X **8**, 031079 (2018).
[12] T. E. Lee, Anomalous Edge State in a Non-Hermitian Lattice, Phys. Rev. Lett. **116**, 133903 (2016).
[13] Y. Takasu, T. Yagami, Y. Ashida, R. Hamazaki, Y. Kuno, and Y. Takahashi, PT-symmetric non-Hermitian quantum many-body system using ultracold atoms in an optical lattice with controlled dissipation, Prog. Theor. Exp. Phys. **2020**, 12A110 (2020).
[14] M. Fruchart, R. Hanai, P. B. Littlewood, and V. Vitelli, Non-reciprocal phase transitions, Nature (London) **592**, 363 (2021).
[15] X. Turkeshi and M. Schiró, Entanglement and correlation spreading in non-Hermitian spin chains, Phys. Rev. B **107**, L020403 (2023).
[16] Y. L. Gal, X. Turkeshi, and M. Schiro, Volume-to-area law entanglement transition in a non-Hermitian free fermionic chain, SciPost Phys. **14**, 138 (2023).
[17] C. H. Lee, Exceptional Bound States and Negative Entanglement Entropy, Phys. Rev. Lett. **128**, 010402 (2022).
[18] N. Hatano and D. R. Nelson, Localization Transitions in Non-Hermitian Quantum Mechanics, Phys. Rev. Lett. **77**, 570 (1996).
[19] N. Hatano and D. R. Nelson, Vortex pinning and non-Hermitian quantum mechanics, Phys. Rev. B **56**, 8651 (1997).
[20] L. Feng, R. El-Ganainy, and L. Ge, Non-Hermitian photonics based on parity–time symmetry, Nat. Photonics **11**, 752 (2017).
[21] T. Ozawa, H. M. Price, A. Amo, N. Goldman, M. Hafezi, L. Lu, M. C. Rechtsman, D. Schuster, J. Simon, O. Zilberberg, and I. Carusotto, Topological photonics, Rev. Mod. Phys. **91**, 015006 (2019).

[22] Y. Nagai, Y. Qi, H. Isobe, V. Kozii, and L. Fu, DMFT Reveals the Non-Hermitian Topology and Fermi Arcs in Heavy-Fermion Systems, Phys. Rev. Lett. **125**, 227204 (2020).
[23] S. Yao and Z. Wang, Edge States and Topological Invariants of Non-Hermitian Systems, Phys. Rev. Lett. **121**, 086803 (2018).
[24] F. K. Kunst, E. Edvardsson, J. C. Budich, and E. J. Bergholtz, Biorthogonal Bulk-Boundary Correspondence in Non-Hermitian Systems, Phys. Rev. Lett. **121**, 026808 (2018).
[25] A. N. Poddubny, Interaction-induced analog of a non-Hermitian skin effect in a lattice two-body problem, Phys. Rev. B **107**, 045131 (2023).
[26] C. H. Lee, Many-body topological and skin states without open boundaries, Phys. Rev. B **104**, 195102 (2021).
[27] T. Fukui and N. Kawakami, Breakdown of the Mott insulator: Exact solution of an asymmetric Hubbard model, Phys. Rev. B **58**, 16051 (1998).
[28] L. Mao, Y. Hao, and L. Pan, Non-Hermitian skin effect in a one-dimensional interacting Bose gas, Phys. Rev. A **107**, 043315 (2023).
[29] B. Dóra and C. P. Moca, Full counting statistics in the many-body Hatano-Nelson model, Phys. Rev. B **106**, 235125 (2022).
[30] S.-B. Zhang, M. M. Denner, T. Bzdušek, M. A. Sentef, and T. Neupert, Symmetry breaking and spectral structure of the interacting Hatano-Nelson model, Phys. Rev. B **106**, L121102 (2022).
[31] F. Alsallom, L. Herviou, O. V. Yazyev, and M. Brzezińska, Fate of the non-Hermitian skin effect in many-body fermionic systems, Phys. Rev. Res. **4**, 033122 (2022).
[32] E. Lee, H. Lee, and B.-J. Yang, Many-body approach to non-Hermitian physics in fermionic systems, Phys. Rev. B **101**, 121109(R) (2020).
[33] R. Hamazaki, K. Kawabata, and M. Ueda, Non-Hermitian Many-Body Localization, Phys. Rev. Lett. **123**, 090603 (2019).
[34] S. Mu, C. H. Lee, L. Li, and J. Gong, Emergent Fermi surface in a many-body non-Hermitian fermionic chain, Phys. Rev. B **102**, 081115(R) (2020).
[35] D.-W. Zhang, Y.-L. Chen, G.-Q. Zhang, L.-J. Lang, Z. Li, and S.-L. Zhu, Skin superfluid, topological Mott insulators, and asymmetric dynamics in an interacting non-Hermitian Aubry-André-Harper model, Phys. Rev. B **101**, 235150 (2020).
[36] Z. Wang, L.-J. Lang, and L. He, Emergent Mott insulators and non-Hermitian conservation laws in an interacting bosonic chain with noninteger filling and nonreciprocal hopping, Phys. Rev. B **105**, 054315 (2022).
[37] R. Shen and C. H. Lee, Non-Hermitian skin clusters from strong interactions, Commun. Phys. **5**, 238 (2022).
[38] T. Yoshida and Y. Hatsugai, Reduction of one-dimensional non-Hermitian point-gap topology by interactions, Phys. Rev. B **106**, 205147 (2022).
[39] K. Kawabata, T. Numasawa, and S. Ryu, Entanglement Phase Transition Induced by the Non-Hermitian Skin Effect, Phys. Rev. X **13**, 021007 (2023).
[40] C. M. Bender, Making sense of non-Hermitian Hamiltonians, Rep. Prog. Phys. **70**, 947 (2007).
[41] K. Yamamoto, M. Nakagawa, M. Tezuka, M. Ueda, and N. Kawakami, Universal properties of dissipative Tomonaga-Luttinger liquids: Case study of a non-Hermitian xxz spin chain, Phys. Rev. B **105**, 205125 (2022).
[42] I. Affleck, W. Hofstetter, D. R. Nelson, and U. Schollwöck, Non-Hermitian Luttinger liquids and flux line pinning in planar superconductors, J. Stat. Mech.: Theory Exp. (2004) P10003.
[43] W. Hofstetter, I. Affleck, D. Nelson, and U. Schollwöck, Non-Hermitian Luttinger liquids and vortex physics, Europhys. Lett. **66**, 178 (2004).
[44] K. Yamamoto and N. Kawakami, Universal description of dissipative Tomonaga-Luttinger liquids with SU(n) spin symmetry: Exact spectrum and critical exponents, Phys. Rev. B **107**, 045110 (2023).
[45] U. Schollwöck, The density-matrix renormalization group in the age of matrix product states, Ann. Phys. **326**, 96 (2011).
[46] G. Vidal, Classical Simulation of Infinite-Size Quantum Lattice Systems in One Spatial Dimension, Phys. Rev. Lett. **98**, 070201 (2007).
[47] T. Giamarchi, *Quantum Physics in One Dimension* (Oxford University Press, Oxford, England, 2004).
[48] M. A. Cazalilla, Bosonizing one-dimensional cold atomic gases, J. Phys. B: At., Mol. Opt. Phys. **37**, S1 (2004).
[49] A. O. Gogolin, A. A. Nersesyan, and A. M. Tsvelik, *Bosonization and Strongly Correlated Systems* (Cambridge University Press, Cambridge, England, 1998).
[50] J.-S. Bernier, R. Citro, C. Kollath, and E. Orignac, Correlation Dynamics During a Slow Interaction Quench in a One-Dimensional Bose Gas, Phys. Rev. Lett. **112**, 065301 (2014).
[51] M. A. Cazalilla, R. Citro, T. Giamarchi, E. Orignac, and M. Rigol, One dimensional bosons: From condensed matter systems to ultracold gases, Rev. Mod. Phys. **83**, 1405 (2011).
[52] M. A. Cazalilla, Effect of Suddenly Turning on Interactions in the Luttinger Model, Phys. Rev. Lett. **97**, 156403 (2006).
[53] J. von Delft and H. Schoeller, Bosonization for beginners – Refermionization for experts, Ann. Phys. (Leipzig) **510**, 225 (1998).
[54] J. Lancaster and A. Mitra, Quantum quenches in an *xxz* spin chain from a spatially inhomogeneous initial state, Phys. Rev. E **81**, 061134 (2010).
[55] I. Gradshteyn and I. Ryzhik, *Table of Integrals, Series, and Products* (Academic Press, New York, 2007).
[56] H. Schomerus and J. Wiersig, Non-Hermitian-transport effects in coupled-resonator optical waveguides, Phys. Rev. A **90**, 053819 (2014).
[57] E. M. Graefe, H. J. Korsch, and A. E. Niederle, Mean-Field Dynamics of a Non-Hermitian Bose-Hubbard Dimer, Phys. Rev. Lett. **101**, 150408 (2008).
[58] H. Carmichael, *An Open Systems Approach to Quantum Optics* (Springer-Verlag, Berlin, 1993).
[59] A. J. Daley, Quantum trajectories and open many-body quantum systems, Adv. Phys. **63**, 77 (2014).
[60] S. R. White, Density Matrix Formulation for Quantum Renormalization Groups, Phys. Rev. Lett. **69**, 2863 (1992).